

Strain relaxation in buried SrRuO₃ layer in (Ca_{1-x}Sr_x)(Zr_{1-x}Ru_x)O₃/SrRuO₃/SrTiO₃ system

Soo Gil Kim, Yudi Wang, and I-Wei Chen^{a)}

Department of Materials Science and Engineering, University of Pennsylvania, Philadelphia, Pennsylvania 19104

(Received 17 April 2006; accepted 25 May 2006; published online 18 July 2006)

A novel relaxation phenomenon occurs in buried SrRuO₃ layers in strained (Ca_{1-x}Sr_x)(Zr_{1-x}Ru_x)O₃/SrRuO₃/SrTiO₃ (001) thin film system. The lightly strained SrRuO₃ buried layer is initially clamped by the SrTiO₃ substrate. After a heavily strained (Ca_{1-x}Sr_x)(Zr_{1-x}Ru_x)O₃ overlayer is deposited, localized strain relaxation develops in the buried layer. This is manifested by a crosshatch pattern of <100> corrugations on the surface, due to the slip of <110> {110} threading dislocations. The phenomenon can be controlled by tuning the growth kinetics and strain energy of the overlayer. © 2006 American Institute of Physics.

[DOI: 10.1063/1.2221900]

Thin films grown on lattice-mismatched substrates can undergo strain relaxation by generating threading and misfit dislocations.^{1,2} Subsequently, film surfaces develop a crosshatch topography reflecting dislocation slip traces undergoing diffusional smoothing.^{3,4} In (100) III-V semiconductor layers on (100) substrates (e.g., InGaAs/GaAs, SiGe/Si), <110> dislocations on {111} slip planes leave <110> surface traces arranged in a 90° crosshatch grid pattern.^{1,5-8} Crosshatch morphology has also been reported for SrRuO₃ (SRO) films deposited on (100) oriented SrTiO₃ (STO) substrates (misfit strain $\epsilon_m=0.64\%$), but only in thick films (320 nm) after postdeposition annealing (8 h at 650 °C).⁹ Here we report the first observation of crosshatch development which relaxes a lightly strained buried layer (SRO) burdened by a heavily strained overlayer [SRO-alloyed CaZrO₃ (CZO)]. The relaxation occurs via <110> {110} dislocations.

Multilayer (CZO)_{1-x}(SRO)_x/SRO/STO films were grown on (001) STO substrates by laser ablation deposition using a KrF laser ($\lambda=248$ nm) emitting ~200 mJ pulses. The substrates (with a miscut angle $\approx 0.3^\circ$) were prepared per Refs. 10 and 11 to provide TiO₂-terminated surfaces with steps of a unit cell height (0.4 nm). A 20 nm STO layer was first deposited at 700 °C in 100 mTorr O₂ which grew in a step-flow manner. Next, SRO was grown under the same condition to a thickness (δ_b) of 30 nm, which was too thin to cause strain relaxation during either deposition or postdeposition annealing (e.g., 650 °C for 1 h). Finally, an overlayer of (Ca_{1-x}Sr_x)(Zr_{1-x}Ru_x)O₃ of various thicknesses (δ_o) and compositions (x) was deposited at various temperatures (T) and O₂ pressures (P) to impart additional strain energy to the (Ca_{1-x}Sr_x)(Zr_{1-x}Ru_x)O₃/SRO/STO system. The film thickness, lattice parameters, and full width at half maximum (FWHM) of the crystal orientations [e.g., ω scan of (002) reflection of SRO] were determined by a four-circle x-ray diffractometer (Bruker-AXS D8) using a Cu $K\alpha$ source. The surface morphology was observed by atomic force microscopy (AFM).

The as-grown SRO film has a step-and-terrace structure [Fig. 1(a)]. Its out-of-plane lattice parameter (c_b), 0.3954 nm

determined from Fig. 2(a), is larger than the stress-free lattice parameter (0.3930 nm) indicating a state of in-plane compressive strain (ϵ_b) set to match the substrate STO lattice parameter (0.3905 nm). Despite the strain, the FWHM of SRO (002) plane, 0.05°, is only slightly higher than that of the substrate (0.03°). So the SRO film was probably clamped and not yet relaxed. The subsequent overlayer deposition may take either a two-dimensional (2D) or a three-dimensional (3D) island-growth mode. Under the latter condition (e.g., $P \geq 10^{-2}$ Torr, $T=650$ °C), the buried SRO film

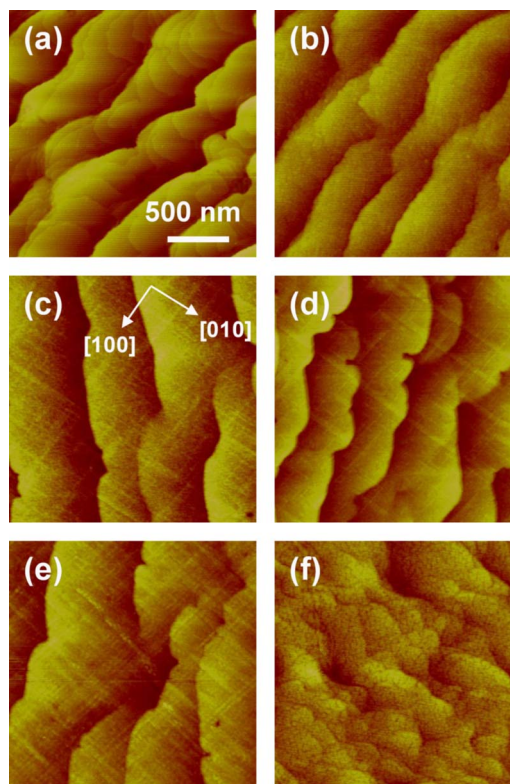


FIG. 1. (Color online) AFM images of (a) SrRuO₃ on SrTiO₃ (001) substrate, with additional (Ca_{0.93}Sr_{0.07})(Zr_{0.93}Ru_{0.07})O₃ overlayer deposited at (b) 650 °C/10 mTorr to 20 nm, (c) 650 °C/1 mTorr to 20 nm, (d) 650 °C/1 mTorr to 10 nm, and (e) 650 °C/1 mTorr to 30 nm, or with (f) additional 20 nm CaZrO₃ overlayer deposited at 650 °C/10⁻⁶ Torr.

^{a)}Electronic mail: iweichen@seas.upenn.edu

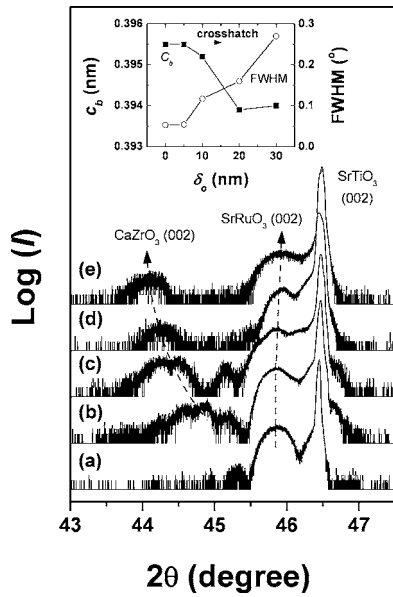


FIG. 2. (Color online) XRD patterns of (a) SrRuO₃ on SrTiO₃ (001) and (Ca_{0.93}Sr_{0.07})(Zr_{0.93}Ru_{0.07})O₃/SrRuO₃/SrTiO₃ (100) deposited at 650 °C in (b) 100 mTorr, (c) 10 mTorr, (d) 1 mTorr, and (e) 10⁻⁶ Torr O₂. Peak at ~45.2° is satellite of SrRuO₃ (002) reflection. Inset: out-of-plane lattice parameter and FWHM of rocking curve of SrRuO₃ buried layer vs overlayer [(Ca_{0.93}Sr_{0.07})(Zr_{0.93}Ru_{0.07})O₃, 650 °C/1 mTorr] thickness. Note abrupt change upon forming crosshatch.

typically showed a little change in c_b [Figs. 2(b) and 2(c)], and the surface morphology remained flat [Fig. 1(b)]. In contrast, under the former condition (e.g., $P \leq 10^{-3}$ Torr, $T = 650$ °C), the buried film often showed a c_b reduction [Figs. 2(d) and 2(e)], together with the development of a crosshatch surface pattern [Fig. 1(c)]. This suggests that crosshatch is associated with the 2D growth of a coherent overlayer which strains the system to the point of triggering relaxation in the buried layer, whereas the 3D growth of an overlayer has little effect.

To further substantiate the above claim, we have investigated the overlayer deposition under a wide range of conditions (x , δ_o , T , and P), and documented the crosshatch observation, growth modes, and the strains in the overlayer and buried layer. Since the in-plane strain of the overlayer ε_o is related to the out-of-plane strain, $\varepsilon_o' = -2\nu\varepsilon_o/(1-\nu)$, where ν is the Poisson's ratio, we can evaluate ε_o' by $\varepsilon_o' = (c_o/c_{oo}) - 1$, where c_o is the out-of-plane lattice parameter of the overlayer, and c_{oo} its stress-free value [c_{oo} (nm) = 0.4012(1- x) + 0.3930 x , given CZO lattice parameter = 0.4012 nm]. The correlations to $\delta_o\varepsilon_o'$ of the overlayer are shown in Fig. 3 for P , T , and the c_b and FWHM of the buried layer. In all cases, it is apparent that (a) crosshatch never develops in 3D growth, (b) $\delta_o\varepsilon_o' > 0.4$ nm is required for crosshatch to form in 2D growth, and (c) both c_b and FWHM of the buried layer are constant for $\delta_o\varepsilon_o' < 0.4$ nm, but c_b decreases and FWHM increases for $\delta_o\varepsilon_o' > 0.4$ nm. (A subset of the latter correlation is shown for δ_o variation in Fig. 2 inset; similar observations were also made when P , T , or x were varied.) A causal relation between crosshatch formation, growth mode, and the $\delta_o\varepsilon_o'$ of the overlayer is thus established.

Several points are noteworthy. First, the 2D/3D growth mode transition typically took place at high P and low T [Figs. 3(a) and 3(b)], corresponding to a relatively low ki-

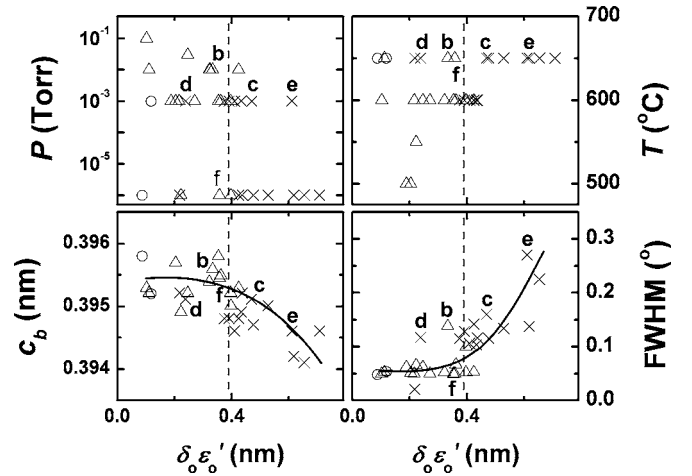


FIG. 3. (Color online) Strain (ε_o') thickness (δ_o) of overlayer correlated to growth mode and crosshatch formation (x: crosshatch in 2D growth, o: no crosshatch in 2D growth, Δ: no crosshatch in 3D growth) at various deposition pressures P and temperatures T , yielding various out-of-plane lattice parameters c_b and FWHMs for SrRuO₃ buried layer. Letters b-f refer to same films in Figs. 1(b)–1(f).

netic energy of incoming atoms and low thermal energy of adatoms, respectively. Since in 3D growth the side surfaces of islands are free of constraint, the overlayer can elastically relax despite clamping by the buried layer beneath, thus adding little driving force for strain relaxation. Second, as crosshatch develops at lower P and higher T , its grid spacing (l) decreases with $\delta_o\varepsilon_o'$; e.g., as δ_o increases from 10 to 30 nm ($\delta_o\varepsilon_o'$ from 0.239 to 0.611 nm) l decreases from 218 to 120 nm [Fig. 1(d) and 1(e)] indicating more strain relaxation in thicker film.¹² Third, although c_{oo} increases with decreasing x , the excessive mismatch of CZO ($\varepsilon_m = 2.67\%$) films cannot be supported by the overlayer in coherent growth, resulting in a 2D/3D growth transition. [Fig. 1(f), where ε_o of the CZO layer is only 1%.] Lastly, despite the preponderance of crosshatch formation in the present study, it was possible to grow a highly strained crosshatch-free overlayer (e.g., $x = 0.1$, $\delta_o = 20$ nm, and $\delta_o\varepsilon_o' = 0.39$ nm) by using relatively low T and high P (e.g., 625 °C/10⁻³ Torr or 600 °C/10⁻⁴ Torr), conditions at the border of 2D/3D growth mode yet giving relatively smooth surfaces.

According to x-ray diffraction, the crosshatch grid aligns along $\langle 100 \rangle$ [Fig. 1(c)]. This is consistent with the operation of $\langle 110 \rangle \{110\}$ dislocations, a dominant slip system in perovskites,^{13–15} depicted in Fig. 4 inset with a $[010]$ slip trace and a dislocation with a Burgers vector b of 0.552 nm. Using the method of Freund^{16,17} and assuming a uniform shear modulus μ in the entire system, we can write the driving force G on threading dislocation advance as

$$G = 2\mu b(\delta_o\varepsilon_o + \delta_b\varepsilon_b)\sin\alpha\sin\beta\left(\frac{1+\nu}{1-\nu}\right) - \frac{\mu b^2\sin^2\beta}{4\pi(1-\nu)}\left\{\frac{(1-\nu\cos^2\beta)}{\sin^2\beta}\ln\left[\frac{2(\delta_o+\delta_b)}{r_o}\right] - \frac{1}{2}\cos 2\alpha + \frac{1-2\nu}{4(1-\nu)}\right\}. \quad (1)$$

Here, the misfit forces due to the overlayer ($\propto \delta_o\varepsilon_o$) and the buried layer ($\propto \delta_b\varepsilon_b$, ε_b =misfit strain in SRO) are countered by the self-force of the dislocation with a core radius r_o with

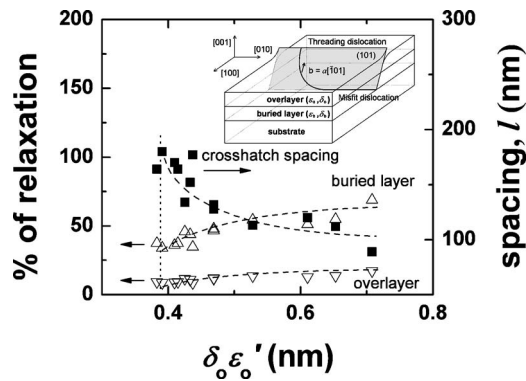


FIG. 4. (Color online) Measured crosshatch spacing (l) and percent of strain relaxation of buried and overlayer as a function of $\delta_o \epsilon_o'$. Inset: slip geometry of threading and misfit dislocation.

angles α (between the slip plane and the film normal) being 45° and β (between the Burgers vector and the slip-plan/substrate intersection) being 90° . This equation correctly predicts a higher driving force as $\delta_o \epsilon_o$ in the overlayer increases, but the predicted critical $\delta_o \epsilon_o'$ (or $\delta_o \epsilon_o' = 1.17 \delta_o \epsilon_o$ for $\nu=0.3$) underestimates the observed value (Fig. 3) by about a factor of 10. Such disagreement is also found in III-V semiconductors (e.g., see Fig. 2 of Ref. 3) and may be attributed to the additional driving force needed to overcome dislocation interactions.^{16,17} This is not surprising since each crosshatch step is typically 1–3 nm high, indicating the passage of more than one dislocation.

For $\langle 110 \rangle$ misfit dislocation, a grid of $l = b \sin \alpha / \epsilon_b = 61.4$ nm is required to fully relax the SRO layer, versus $l = 15.4$ nm to fully relax an overlayer ($\epsilon_o \sim 2.53\%$). In this study, the smallest l was 89 nm at $\delta_o \epsilon_o' = 0.65$ nm, which would provide 70% relaxation in the SRO layer but only 20% in the overlayer. The amount of strain relaxation in crosshatched samples, estimated using the ratio of the required l to actual l , is shown in Fig. 4. It makes clear that while crosshatch provides a visual signature of slip relaxation, the relaxation is mostly concentrated to the buried layer.

In summary, a novel geometry to reveal crosshatch without full strain relaxation was used to establish the strain relaxation mechanism in perovskite heterostructures. Crosshatch occurs during the 2D growth of a strained overlayer,

involving $\langle 110 \rangle$ threading dislocations gliding on the $\{101\}$ planes from the surface to the substrate, relaxing the buried layer but leaving most misfit strain in the overlayer intact. Visual and x-ray diffraction studies then allow an accurate determination of the relaxation condition and the dislocation system without thin-film microscopy that might alter the dislocation configurations. Crosshatch development is controlled by the growth kinetics and the strain energy of the overlayer. In a narrow processing window of mixed 2D/3D growth smooth heterostructures without crosshatch can be obtained.

This work was supported by the U.S. National Science Foundation, Grant Nos. DMR 03-03458 and DMR05-20020, and Korea Research Foundation, Grant No. KRF-2004-214-D00308 (S.G.K.).

- ¹J. W. Matthews and A. E. Blakeslee, *J. Cryst. Growth* **27**, 118 (1974).
- ²J. W. Matthews, *J. Vac. Sci. Technol.* **12**, 126 (1975).
- ³A. M. Andrews, J. S. Speck, A. E. Romanov, M. Bobeth, and W. Pompe, *J. Appl. Phys.* **91**, 1933 (2002).
- ⁴A. M. Andrews, R. LeSar, M. A. Kerner, J. S. Speck, A. E. Romanov, A. L. Kolesnikova, M. Bobeth, and W. Pompe, *J. Appl. Phys.* **95**, 6032 (2004).
- ⁵T. Nishioka, Y. Itoh, A. Yamamoto, and M. Yamaguchi, *Appl. Phys. Lett.* **51**, 1928 (1987).
- ⁶K. H. Chang, R. Gibala, D. J. Srolovitz, P. K. Bhattachaya, and J. F. Mansfield, *J. Appl. Phys.* **67**, 4093 (1990).
- ⁷S. Y. Shiryayev, P. Jensen, and J. W. Peterson, *Appl. Phys. Lett.* **64**, 3305 (1994).
- ⁸A. M. Andrews, A. E. Romanov, J. S. Speck, M. Bobeth, and W. Pompe, *Appl. Phys. Lett.* **77**, 3740 (2000).
- ⁹F. Sánchez, M. V. García-Cuenca, C. Ferrater, M. Varela, G. Herranz, B. Martínez, and J. Fontcuberta, *Appl. Phys. Lett.* **83**, 902 (2003).
- ¹⁰M. Kawasaki, K. Takahashi, T. Maeda, R. Tsuchiya, M. Shinohara, O. Ishiyama, T. Yonezawa, M. Yoshimoto, and H. Koinuma, *Science* **266**, 1540 (1994).
- ¹¹G. Koster, B. L. Kropman, G. J. H. M. Rijnders, D. H. A. Blank, and H. Rogalla, *Appl. Phys. Lett.* **73**, 2920 (1998).
- ¹²H. P. Sun, W. Tian, X. Q. Pan, J. H. Haeni, and D. G. Schlom, *Appl. Phys. Lett.* **84**, 3298 (2004).
- ¹³T. E. Mitchell and A. H. Heuer, in *Dislocation in Solids*, edited by F. R. N. Nabarro and J. P. Hirth (Elsevier, New York, 2004), Vol. 12, Chap. 68, p. 375.
- ¹⁴S. H. Oh and C. G. Park, *J. Appl. Phys.* **95**, 4691 (2004).
- ¹⁵J. S. Speck and W. Pompe, *J. Appl. Phys.* **76**, 466 (1994).
- ¹⁶L. B. Freund, *J. Mech. Phys. Solids* **38**, 657 (1990).
- ¹⁷L. B. Freund, *MRS Bull.* **17**, 52 (1992).